Supporting Information

Berdichevski et al. 10.1073/pnas.1502232112

SI PF-GdDTPA-Cy5.5 Biopolymer Preparation and Implantation

PF precursor solution (1) was labeled with Gd and Cy5.5 to provide MR and fluorescence contrast, respectively. PEG-DA (0.25–0.5%) was added to retain the degree of cross-linking as measured by shear modulus, G′ (range of 120 ± 60 Pa). Irgacure 2959 photoinitiator (Ciba Specialty Chemicals) was added (0.1% wt/vol) to the pregel solution. The chemical makeup of the labeled PF hydrogels is illustrated in Fig. S3*A*. Each of the three configurations (i.e., 5-mm-diameter preformed cylindrical plugs, 200- to 500-μm-diameter preformed injectable spherical microbeads, or hydrogel precursor injected and polymerized in situ) with the initial volume of 250 μL were implanted as described in *SI Materials and Methods*. Fig. S3*B* demonstrates a schematic illustration of the implantation strategies used in the study.

SI Validation of Hydrogel Labeling for Fluorescence and MRI

For MRI contrast, the Gd (III) ion was immobilized in the hydrogels using a diethylene triamine pentaacetic acid (DTPA) chelator (2), which reduces the lanthanide's toxicity to mammalian cells and renders it safe for clinical application (3–6). An in vitro assay was used to calibrate the amount of contrast agent required for in vivo MR imaging. An increase in the concentration of Gd-labeled molecules results in a shortening of the relaxation time T1 (7, 8), and therefore in the elevation of the relaxation rate R1 (defined as 1/T1). This effect is clearly demonstrated at Fig. S1 *A* and *B*. We verified that the correlation between the contrast agent concentration and the R1 values at the investigated range was linear. Typical preparation of PF-GdDTPA resulted in 24 GdDTPA moieties per fibrinogen and relaxivity (defined as the correlation coefficient of R1 vs. Gd concentration) of 14.8 $mM^{-1}{\cdot}s^{-1}$. Further, we determined that the transfer from the solution form to the cross-linked form of the PF hydrogel had an only slight effect on the MR signal (relaxivity of 11.1 $mM^{-1}{\cdot}s^{-1}$; Fig. S1*B*). Based on these experiments, the PF-GdDTPA concentration range used when forming the hydrogel constructs was set to 1.5 ± 0.5 mg/mL. The contrast between the labeled and unlabeled PF was verified using a gel-in-gel assay as detailed below. Two primary configurations were imaged by MR: unlabeled plugs containing labeled microbeads and labeled plugs containing unlabeled microbeads. In both configurations, microbeads appeared intact in terms of their shape. Moreover, there was no evidence of diffusion of free Gd from the labeled to the unlabeled gels (Fig. S1*C*). To reveal whether MR imaging followed by volume measurements using ImageJ is suitable to follow up the labeled hydrogel degradation, precast plug hydrogel constructs with known volume were imaged and measured. Fig. S1*D* clearly demonstrates that the correlation between the actual plug volume and the MRI-measured plug volume was linear with a slope of unity.

For the fluorescence contrast, a Cy5.5-N-hydroxysuccinimide (NHS) label was reacted with nucleophiles on the PF solution to release the NHS groups and create stable amide and imide bonds with primary or secondary amines on the protein. Calculations of the degree of labeling revealed that an average of 4.5 molecules of Cy5.5 were conjugated to every fibrinogen molecule. An in vitro assay was used to calibrate the amount of fluorescence contrast agent required for whole-animal in vivo imaging. Cylindrical plugs were prepared with increasing fluorophore concentration by diluting PF-Cy5.5 with unlabeled PF (Fig. S1*E*). An IVIS200 system was used to detect the fluorescence signal from the plugs, and the intensity was quantified by image analysis. The increased signal intensity associated with higher amounts PF-Cy5.5 in the hydrogels was linearly proportional to the increased concentration up to a saturation point where 67% of the PF was fluorescently labeled (Fig. S1*F*). A slight decrease in the fluorescence signal was observed when the concentration of PF-Cy5.5 went above 67%. We speculate that self-absorption, which occurs when emitted photons excite other molecules in the ground state, was the cause for the reduction in fluorescence (9, 10). A working concentration of 50% PF-Cy5.5 was chosen based on the calibration curves.

SI Cell Compatibility of PF-GdDTPA

Viability and proliferation assays were conducted to investigate toxicity and cell compatibility of the paramagnetic-labeled hydrogels. Fibroblasts were seeded and cultured within microbead hydrogels containing PF-GdDTPA; the cells were stained with calcein/ethidium and imaged fluorescently. A vast majority of cells were alive and only a few dead cells were detected in the center of the microbeads (Fig. S2*A*). The fibroblasts were morphologically elongated and highly spindled and formed interconnections within the PF-GdDTPA hydrogels. Quantitative cell viability was performed on fibroblasts taken from the hydrogels after 1 wk in culture, using a collagenase digestion to dissociate the constructs. A Trypan Blue assay was applied to count the number of viable cells recovered from the dissociated PF-GdDTPA microbeads. The cell viability in PF hydrogels was ∼85–90%, and was not reduced in the presence of Gd (III) (Fig. S2*B*). Proliferation was evaluated using flow cytometry with cell cycle analysis; the fibroblasts in the PF-GdDTPA hydrogels maintained proliferation levels similar to those of cells in PF hydrogels (Fig. S2*C*). Both quantitative viability and proliferation data of the PF-GdDTPA hydrogels were in close agreement with our previous findings on fibroblasts in PF hydrogels (11–13).

SI Materials and Methods

In Vitro MR Imaging and Data Analysis. For the in vitro studies, MR images were acquired using a 9.4 T Biospec spectrometer (Bruker) using a quadrature RF volume coil. Multislice and multiecho sequence were used (varying T_R values: 5, 2, 1, 0.8, 0.7, 0.6, 0.5, 0.4, 0.3, 0.2, 0.1 s, T_E of 11 ms, field of view of 4 × 4 cm, slice thickness of 2 mm, matrix size of 256 × 128 o-fill to 256 × 256, special resolution of 0.156 mm). Images were processed with custom in-house software using MATLAB (The MathWorks, Inc.) to produce pixel-by-pixel R1 maps. For each pixel, R1 (1/T1) was calculated by nonlinear least square fitting to a single exponent: $I = A\,(1 - Be^{-TR/T1})$, where I is the measured signal intensity for each T_R, A is the steady-state signal intensity in fully relaxed images, and B is ∼1 for steady-state saturation. For the in vivo experiments, the images were acquired by experimental animal scanner at 1T (Aspect Imaging), equipped with gradient sets of 500 mT/M. A T1-weighted sequence was used (GRE SP, T_R of 30 ms, T_E of 3.8 ms, field of 35 × 35 mm, slice thickness of 1.5 mm, matrix of 256 × 256, scan dimension was 3D). All of the data were stored as DICOM images and volume of each implant was analyzed with ImageJ software as described elsewhere (14).

Cell Viability and Proliferation. Cell viability was assessed using a live/dead viability assay (Molecular Probes, Inc.) of human foreskin fibroblasts (HFF) (Lonza) encapsulated in hydrogel microbeads. Stained constructs were visualized using Nikon

TE2000 fluorescence microscope with ×4 magnification and imaged with a ProgRes C10 camera (Jenoptik). An FITC filter set was used to image green-stained live cells, and a TRITC filter set was used to visualize red-stained nuclei of dead cells. The red and green images were superimposed to create the final live/dead images. Cell cycle analysis was performed by staining DNA with propidium iodide (PI) (Sigma). The harvesting of the cells from the constructs was done on days 1, 4, and 7 using collagenase type 1A solution (Sigma) for 1 h at 37 °C with mild shaking. The cells in solution were then centrifuged, washed with PBS, and counted with Trypan Blue to assess cell viability. The cells were fixed in 70% (vol/vol) ethanol at 4 °C for 20 min and incubated with PI staining solution for 15 min at 37 °C. The PI fluorescence was acquired by flow cytometry (LSR-II; Becton Dickinson). Viable cells (10,000) were counted and plotted in single-parameter histograms of PI level. Histograms showed three populations, representing cell cycle phases G0/G1, S, and G2/M. Proliferation was quantified as percentage of cells in the S and G2/M phases.

Degree of Labeling Calculation. The ratio of Cy5.5 dye to protein was determined according to Invitrogen's amine-reactive probe labeling protocol. Briefly, we measured the absorbance of PF-Cy5.5 solution (0.2 mg/mL) at 280 nm and the absorbance of the dye at 673 nm. The measured values were inserted into the equation

$$[\text{attached dye}]/[\text{protein}] = \left[A_{\max} \times MW_{\text{protein}}\right] / \left[A_{\text{protein}} \times \varepsilon_{\text{dye}}\right],$$

where A_{max} is the absorbance of the protein–dye conjugate at the emission maxima, $MW_{protein}$ is molecular weight of the fibrinogen (166,000 g/mol), ε_{dye} is extinction coefficient of the dye at its absorbance maximum, and $A_{protein}$ is protein concentration in milligrams per milliliter.

The ratio of Gd to protein was measured by inductively coupled plasma mass spectrometry (ICP-MS). To that end, samples of PF-GdDTPA with known concentrations of the protein were lyophilized, treated with concentrated nitric acid overnight, and then heated in a dry bath for 1 h at 90 °C. After dilution in deionized water, samples were analyzed by ICP-MS against $GdCl_3$ standards. The calculation of the ratio was performed using the following equation:

$$[\text{GdDTPA}]/[\text{protein}] = \left([\text{Gd}]/MW_{\text{Gd}}\right) / \left([\text{protein}]/MW_{\text{protein}}\right),$$

where [Gd] is gadolinium concentration in milligrams per milliliter as measured by ICP-MS, MW_{Gd} is molecular weight of gadolinium (157 g/mol), [protein] is protein concentration in milligrams per milliliter, and $MW_{protein}$ is the molecular weight of fibrinogen.

1. Dikovsky D, Bianco-Peled H, Seliktar D (2008) Defining the role of matrix compliance and proteolysis in three-dimensional cell spreading and remodeling. *Biophys J* 94(7):2914–2925.
2. Hnatowich DJ, Layne WW, Childs RL (1982) The preparation and labeling of DTPA-coupled albumin. *Int J Appl Radiat Isot* 33(5):327–332.
3. Zilkens C, et al. (2012) Three-dimensional delayed gadolinium-enhanced magnetic resonance imaging of hip joint cartilage at 3T: A prospective controlled study. *Eur J Radiol* 81(11):3420–3425.
4. Walz PC, Bush ML, Robinett Z, Kirsch CF, Welling DB (2012) Three-dimensional segmented volumetric analysis of sporadic vestibular schwannomas: Comparison of segmented and linear measurements. *Otolaryngol Head Neck Surg* 147(4):737–743.
5. Zheng J, Allen C, Jaffray D, Chopra A (2004) PEGylated liposome co-encapsulating iohexol and gadoteridol for multimodal CT and MR imaging. *Molecular Imaging and Contrast Agent Database* (National Center for Biotechnology Information, Bethesda).
6. Dafni H, Landsman L, Schechter B, Kohen F, Neeman M (2002) MRI and fluorescence microscopy of the acute vascular response to VEGF165: Vasodilation, hyper-permeability and lymphatic uptake, followed by rapid inactivation of the growth factor. *NMR Biomed* 15(2):120–131.
7. Larsson HB, et al. (1990) Quantitation of blood-brain barrier defect by magnetic resonance imaging and gadolinium-DTPA in patients with multiple sclerosis and brain tumors. *Magn Reson Med* 16(1):117–131.
8. van der Zande M, et al. (2011) In vivo magnetic resonance imaging of the distribution pattern of gadonanotubes released from a degrading poly(lactic-co-glycolic Acid) scaffold. *Tissue Eng Part C Methods* 17(1):19–26.
9. Berlier JE, et al. (2003) Quantitative comparison of long-wavelength Alexa Fluor dyes to Cy dyes: Fluorescence of the dyes and their bioconjugates. *J Histochem Cytochem* 51(12):1699–1712.
10. Gruber HJ, et al. (2000) Anomalous fluorescence enhancement of Cy3 and cy3.5 versus anomalous fluorescence loss of Cy5 and Cy7 upon covalent linking to IgG and noncovalent binding to avidin. *Bioconjug Chem* 11(5):696–704.
11. Gonen-Wadmany M, Goldshmid R, Seliktar D (2011) Biological and mechanical implications of PEGylating proteins into hydrogel biomaterials. *Biomaterials* 32(26):6025–6033.
12. Dikovsky D, Bianco-Peled H, Seliktar D (2006) The effect of structural alterations of PEG-fibrinogen hydrogel scaffolds on 3-D cellular morphology and cellular migration. *Biomaterials* 27(8):1496–1506.
13. Peled E, Boss J, Bejar J, Zinman C, Seliktar D (2007) A novel poly(ethylene glycol)-fibrinogen hydrogel for tibial segmental defect repair in a rat model. *J Biomed Mater Res A* 80(4):874–884.
14. Dello SA, et al. (2007) Liver volumetry plug and play: Do it yourself with ImageJ. *World J Surg* 31(11):2215–2221.

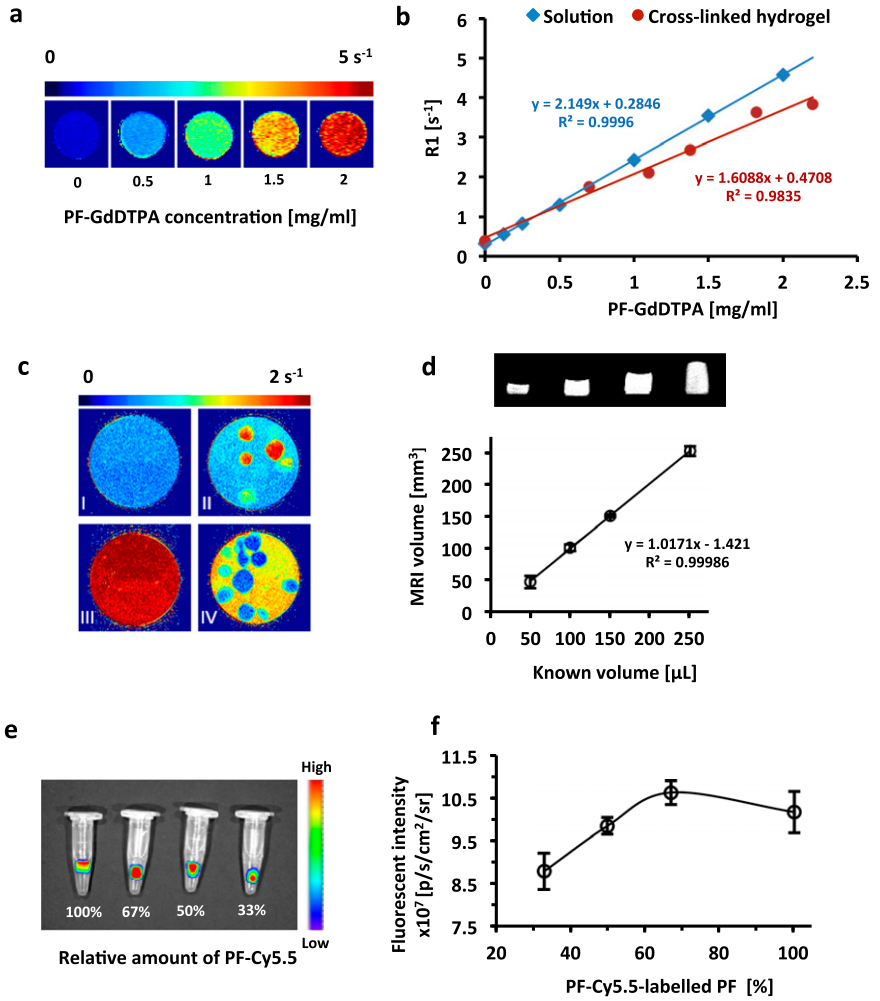

Fig. S1. Validation of hydrogel labeling for fluorescence and MRI. (*A*) R1 relaxivity color map of the PF-GdDTPA in solution. (*B*) R1 values of PF-GdDTPA as a function of the protein concentration in solution and in polymerized hydrogel. (*C*) MRI cross-sectional views of the Gd-labeled and unlabeled plugs cross-linked in different configurations in one tube. The layers are presented as follows: (I) PF hydrogel alone, (II) PF-GdDTPA microbeads in PF outer hydrogel plug, (III) PF-GdDTPA plug, and (IV) PF microbeads in a PF-GdDTPA hydrogel plug. (*D*) The MR image (*Top*) and a calibration graph (*Bottom*) of the PF-GdDTPA hydrogels show the relationship between the known volume and the measured volume of the plugs. (*E*) Fluorescence signal intensity of PF plugs made with decreasing concentrations of PF-Cy5.5 is documented with an IVIS200 system. (*F*) A quantitative relationship between PF-Cy5.5 content and the fluorescence signal; a linear relationship is observed below a certain relative concentration of PF-Cy5.5 (i.e., 67%); mean values are presented with SD.

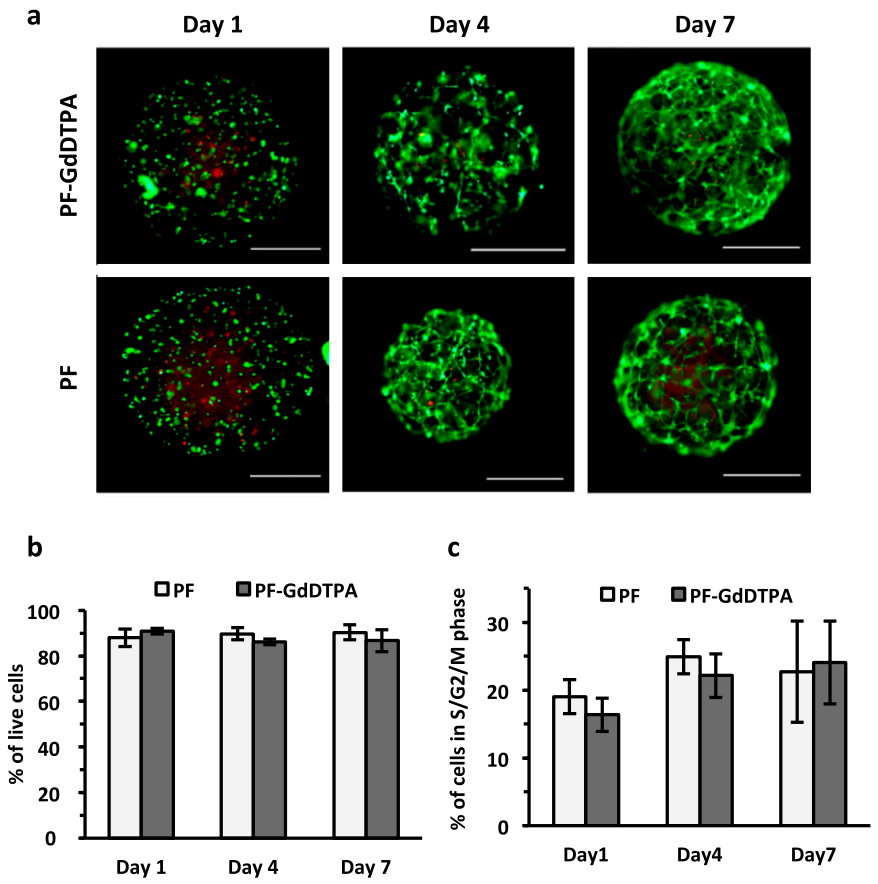

Fig. S2. Cellular compatibility of PF-GdDTPA. (*A*) HFF viability as assessed by calcein (green) and ethidium (red) live/dead staining. (Scale bars, 250 μm.) (*B*) The percent of viable fibroblasts was quantitatively assessed using a Trypan Blue staining assay. (*C*) The proliferation of fibroblasts was quantified using flow cytometry; cells in the S (synthesis), G2, and M (mitosis) phases were considered proliferating. Mean values are shown with SD; $n = 3–5$.

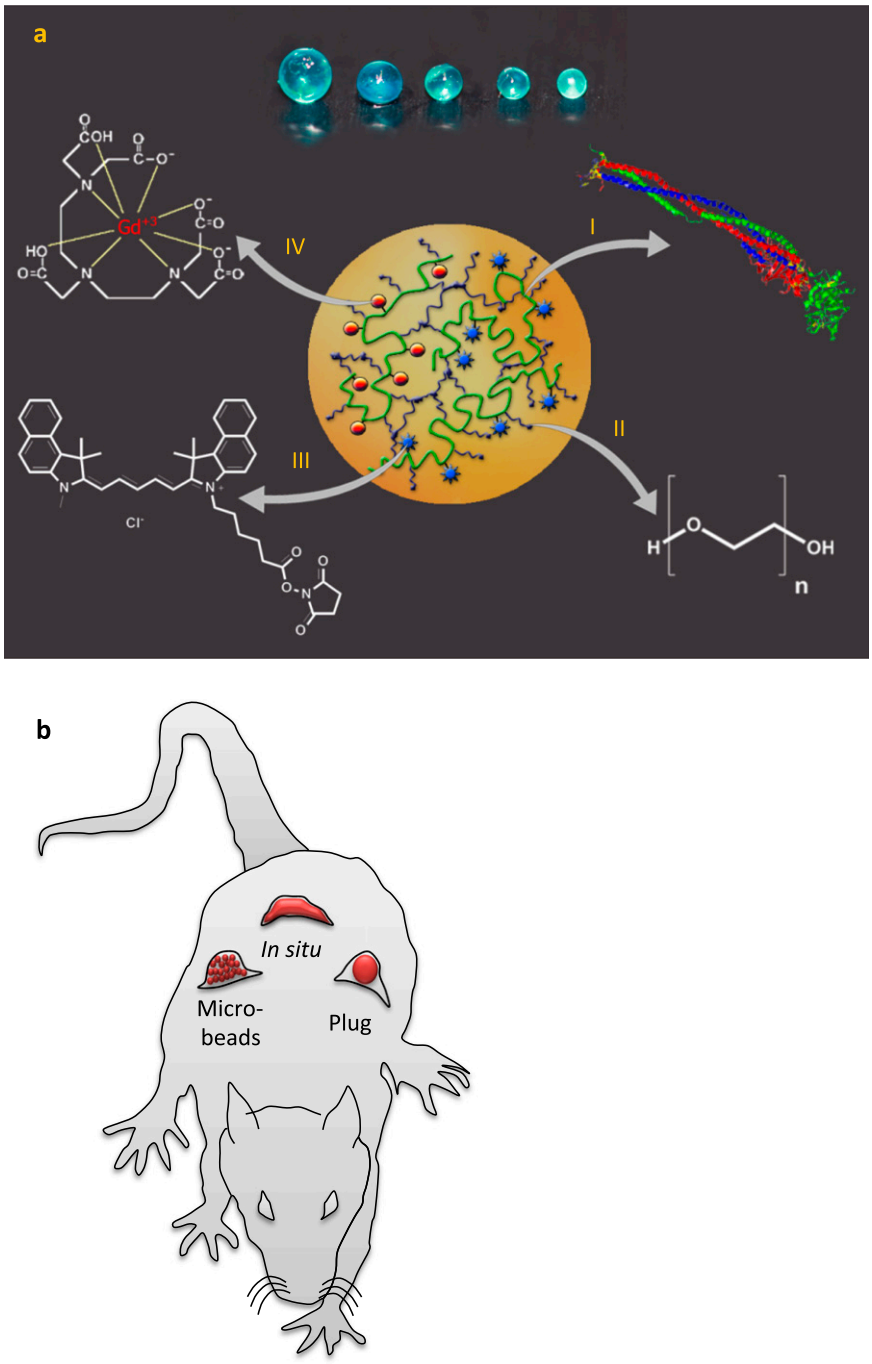

Fig. S3. PF-GdDTPA-Cy5.5 biopolymer preparation and implantation. (*A*) Picture (top) and schematic illustration of the preparation (bottom). A picture of the cross-linked PF-GdDTPA-Cy5.5 hydrogel microbeads. Denatured bovine fibrinogen (I) was conjugated to PEG (II) by Michael-type addition reaction. The Cy5.5 dye (III) was linked to the PF solution by reaction of NHS-ester residues on the fluorescent probe with fibrinogen's primary amines. The conjugation of Gd to the PF through DTPA chelator is shown (IV). (*B*) Schematic illustration of the implantation strategies used in the study. Implant groups included preformed cylindrical plugs (5-mm diameter), preformed injectable spherical microbeads (200–500 μm), or hydrogel precursor injected and polymerized in situ.

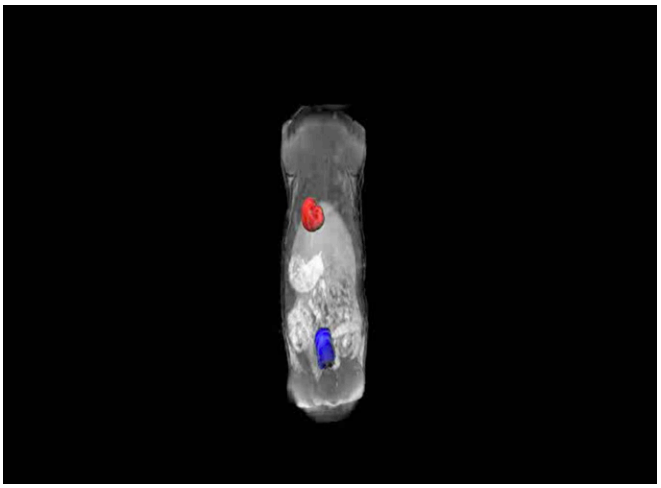

Movie S1. MRI reconstruction of plugs, microbeads, and in situ polymerized hydrogels, inserted s.c. on the backs of Lewis rats at day 0 and after 21 d.

Movie S1